The Ratio of Live Load to Dead Load on I-Girder Prestressed Concrete Bridges Using Theoretical and Numerical Analysis

Rudi Sanjaya, Akhmad Aminullah, Bambang Suhendro

Department of Civil and Environmental Engineering, Gadjah Mada University, Yogyakarta, INDONESIA

E-mail: akhmadaminullah@ugm.ac.id

| Submitted: January 27, 2025 | Revised: February 12, 2025 | Accepted: September 09, 2025 |

| Published: December 31, 2025 |

ABSTRACT

Bridges are essential connectors between regions separated by geographical barriers, facilitating transport across national, provincial, and district roads. In Indonesia, the prestressed I-girder concrete bridge (PCI-Girder) is a widely used design, particularly for spans between 20 and 45 meters. These bridges are a common choice in toll road development projects, part of the national strategic plan to promote regional equity and support economic growth. Seismic loads influence the PCI-Girder bridge superstructure less, allowing consistent design practices concerning cross-sectional dimensions and concrete quality relative to span length. However, girder profiles and spacing variations have become prominent in Indonesia, significantly impacting load distribution and bridge performance. This study examines the effects of live load relative to dead load on PCI-Girder bridges with girder spacing variations of 1850 mm, 2100 mm, and 2450 mm for spans ranging from 20 to 45 meters, based on SNI 1725-2016 standards. Using theoretical calculations in Microsoft Excel and numerical analysis with Midas Civil software, the study highlights the influence of girder spacing on effective area, strand requirements, camber, and beam stress post-tensioning. The findings indicate that increased girder spacing enhances the effective area of composite sections but requires larger strand areas and higher concrete strength. Moment analysis reveals that for spans over 20 meters, dead load moments dominate live load moments, whereas for 20-meter spans, live load moments are more significant. As span length increases, the influence of dead loads becomes more prominent. The 2450 mm spacing variant also shows higher live-to-dead load moment and shear force ratios than other configurations, providing insights for optimizing PCI-Girder bridge designs.

Keywords: I-girder, girder-spacing, strands, toll-road, live-load, dead-load, ratios.

INTRODUCTION

Infrastructure development in Indonesia has seen a significant increase over the past decade. The construction of toll roads and bridges is one of the strategic plans initiated by the government to enhance regional connectivity. According to the Performance Report of the Ministry of Public Works and Housing (PUPR) in the Highway Sector, [1], Indonesia has a total of 19,377 bridge units with a combined length of 562,213.79 meters, achieving a stability rate of over 85%.

Bridges connect between places, routes, or paths separated by geographical factors, whether on national, provincial, or district/city roads. This archipelagic nation has extensively developed various types of bridges and technological advancements. One commonly encountered type is a bridge with a superstructure made of prestressed I-girder concrete, often called PCI-Girder. This type is particularly suitable for bridges with relatively short spans, typically 20 to 45 meters. These bridges are frequently found in toll road construction projects in Indonesia, which are part of the national strategic plan aimed at promoting regional equity to support economic growth. Research by [2], [16] shows that I-girders with a span of 20-45 meters are relatively widely used in Indonesia.

Emphasized the cost-effectiveness of modifying support systems in multi-span bridges to achieve optimal costs. Their research compared four seismic support system modifications using SAP2000 analysis, highlighting that the semi-integral system offered the lowest structural costs. This finding underscores the importance of integrating cost-efficient design modifications at the system level and across individual bridge components [3]. Similarly, [4], [17] explored optimizing PCI-Girder

pISSN 2302-4240
eISSN 2655-2086
Volume 14, Issue 4, December 2025, pp.01074-01090
DOI: http://dx.doi.org/10.32832/astonjadro.v14i4.19037 http://ejournal.uika-bogor.ac.id/index.php/ASTONJADRO

bridges to minimize total costs using the Modified Adaptive Harmony Search Algorithm (MARSHAL). Their findings revealed that PCI-Girder sections designed with the MARSHAL approach achieved superior structural performance compared to those designed using [5], [6] and Caltrans standards. The MARSHAL-optimized sections demonstrated higher structural efficiency factors (ϕ) and better structural behavior ratios (α), signifying the potential of advanced optimization methods in improving PCI-Girder bridge performance.

The superstructure of PCI-Girder bridges is generally less affected by seismic loads, so the design of such bridges should ideally maintain similarities in cross-section dimensions and concrete quality based on the span length. However, as development progresses in Indonesia, numerous differences in design classifications have been observed, particularly in girder profiles and spacing between girders. Varying the spacing between girders typically impacts the load borne by the girder profile, including both live and dead loads. This study examines the influence of live loads relative to dead loads on PCI-Girder bridges with girder spacing variations of 1850 mm, 2100 mm, and 2450 mm for spans ranging from 20 to 45 meters, based on [7] standards. The analysis uses two methods: theoretical calculations using Microsoft Excel and numerical analysis utilizing Midas Civil software.

RESEARCH METHODS

This study uses theoretical and numerical analysis conducted with Midas Civil software to examine toll road bridges with PCI-Girder superstructures. The loading is applied following [7] provisions from the Directorate General of Highways [8], [9].

Further analysis of moment capacity, shear, and deflection is based on the provisions of AASHTO LRFD 2020, [10], and the PCI Design Handbook 7th Edition. The following are several limitations in the design of PCI-Girder bridge superstructures [11]-[15].

1. Allowable concrete stress

The allowable compressive stress of concrete under transfer conditions can be seen in Equation (1). Meanwhile, the allowable tensile stress of concrete under transfer conditions can be seen in Equation (2) for the support location, Equation (3) for places other than the support, and Equation (4) for the joint locations between girder segments.

$$f_{ci} = 0{,}6\, f_{ci}' \quad (1)$$

$$f_{ti} = 0{,}50\, \sqrt{f_{ci}'} \quad \text{(at support)} \quad (2)$$

$$f_{ti} = 0{,}25\, \sqrt{f_{ci}'} \quad \text{(at other than support)} \quad (3)$$

$$f_{ti} = 0 \quad \text{(at joint)} \quad (4)$$

For service conditions, the allowable compressive stress of concrete can be found in Equation (5), while the allowable tensile stress of concrete can be found in Equation (6).

$$f_{cs} = 0{,}45\, f_c' \quad (5)$$

$$f_{ts} = 0{,}50\, \sqrt{f_c'} \quad (6)$$

2. Flexural strength

The nominal flexural strength of prestressed concrete sections, M_n, is calculated using the ultimate strength method. A concrete section is considered to reach a balanced state when the strain in the concrete at the extreme compression fiber reaches $\varepsilon_c = 0{,}003$, while the tensile reinforcement strain corresponds to the yield strain, f_y, for non-prestressed reinforcement and f_{py} for prestressed reinforcement.

Following [10], the ultimate stress in the prestressing steel, f_{ps}, used to determine the nominal strength of a prestressed concrete section, must not exceed f_{py}. If no precise calculations are available, the effective stress in the tendons should meet $f_{se} \geq 0{,}5\, f_{pu}$. For bonded tendons, the value of f_{ps} can be determined using the equation:

$$f_{ps} = f_{pu}\left\{1 - \frac{\gamma_p}{\beta_1}\left[\rho_p \frac{f_{pu}}{f_c'} + \frac{d}{d_p}\frac{f_y}{f_c'}(\rho - \rho')\right]\right\} \quad (7)$$

The design strength must exceed the required strength. The nominal moment strength, Mn, is determined by analyzing the beam under two conditions: as a composite beam and as a non-composite beam.

$$\phi\, Mn \geq Mu \quad (8)$$

3. Shear strength

The nominal shear strength, Vn, must not exceed the combined shear strength contributed by the concrete and the shear reinforcement within the cross-section of the structural component.

$$\phi\, V_n \geq V_u \quad (9)$$

$$V_n = V_c + V_s \quad (10)$$

4. Camber & deflection

Due to the eccentricity of prestressing tendons, prestressed beam elements typically curve upward when the applied external moment is still small. This upward deflection is referred to as camber. The magnitude of the camber may increase or decrease over time. Conversely, external loads acting on the beam will cause downward deflection. In design, the magnitudes of upward and downward deflections must be evaluated and limited to ensure they do not exceed the allowable deflection limits. The following outlines the deflection limits based on [6] and camber tolerances according to the PCI Design Handbook:

Camber due to post-tensioning, $\delta < L/800 \pm L/960$ (11)
Deflection under service conditions without live load, $\delta < 0$ (12)
Deflection under service conditions with live load, $\delta < L/300$ (13)
Deflection due to live load only, $\delta < L/800$ (14)

To simplify the explanation of the methods used in this research, the research flowchart can be seen in **Figure 1**.

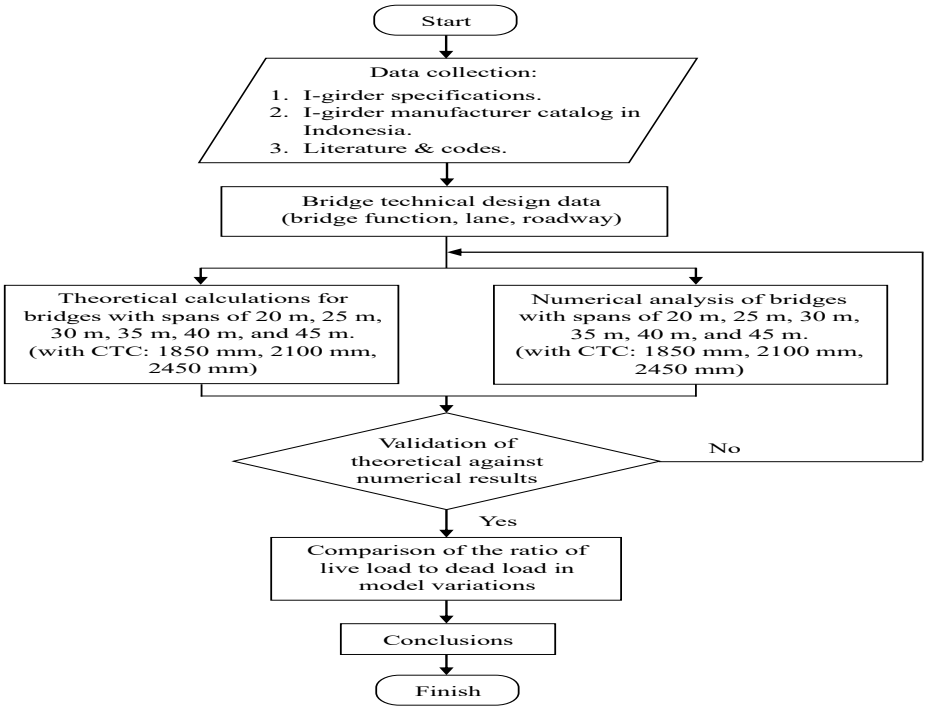

Figure 1. Flow chart

ASTONJADRO
pISSN 2302-4240
eISSN 2655-2086
Volume 14, Issue 4, December 2025, pp.01074-01090
DOI: http://dx.doi.org/10.32832/astonjadro.v14i4.19037 http://ejournal.uika-bogor.ac.id/index.php/ASTONJADRO

Girder cross-section

This study utilizes the available I-girder cross-sections from various manufacturers in Indonesia as references for designing cross-sections for each variation of bridge spans analyzed. The I-girder cross-section in Indonesia is relatively similar to the [5] cross-section but has undergone various modifications. Different manufacturers of I-girders in Indonesia produce cross-sections with varying designs. However, in this study, two manufacturers were selected to represent the available cross-section models in Indonesia. These manufacturers are called "Manufacturer A" and "Manufacturer B".

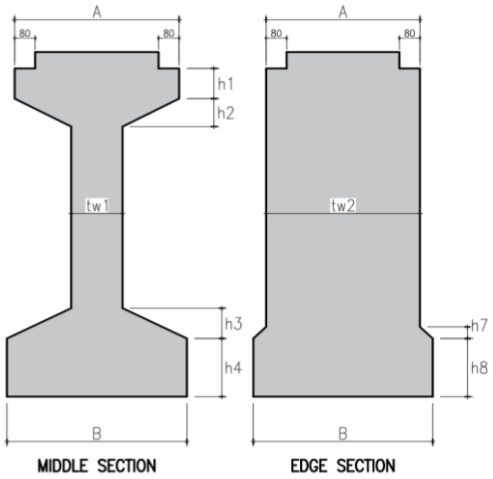

Figure 2. Cross section type-1

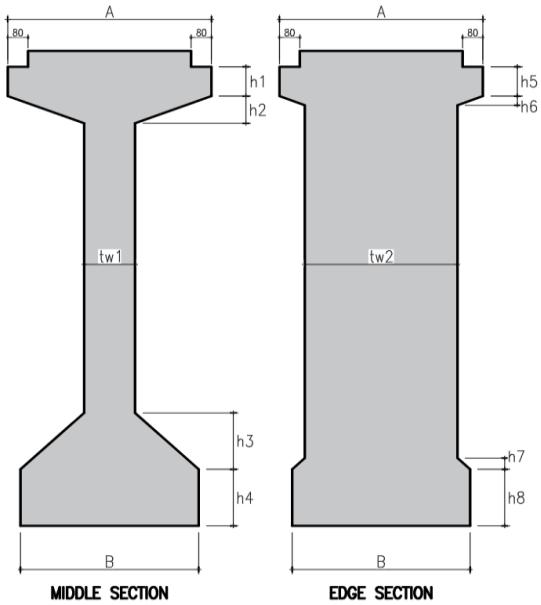

Figure 3. Cross section type-2

Table 1. Cross section of "Manufacturer A" I-girder

Cross section code	H mm	A mm	B mm	Tw1 mm	Tw2 mm	h1 mm	h2 mm	h3 mm	h4 mm	h5 mm	h6 mm	h7 mm	h8 mm
TYPE-1													
A-PCI-H900-170.1	900	350	650	170	550	150	75	100	125	-	-	21	125
A-PCI-H900-170.2	900	350	700	170	550	150	75	100	125	-	-	21	125
A-PCI-H1250-170.1	1250	350	650	170	550	150	75	100	125	-	-	21	125
A-PCI-H1250-170.2	1250	350	700	170	550	150	75	100	125	-	-	21	125
A-PCI-H1600-180.1	1600	550	650	180	550	200	120	100	225	200	22	22	225
A-PCI-H1600-180.2	1600	550	700	180	550	200	120	100	225	200	22	22	225
TYPE-2													
A-PCI-H1700-200.1	1700	800	700	200	600	200	120	250	250	200	40	50	250
A-PCI-H1700-200.2	1700	800	750	200	600	200	120	250	250	200	40	50	250
A-PCI-H2100-200.1	2100	800	700	200	600	200	120	250	250	200	40	50	250

A-PCI-H2100-200.2	2100	800	750	200	600	200	120	250	250	200	40	50	250
A-PCI-H2100-250.1	2100	800	700	250	650	200	120	250	250	200	40	50	250
A-PCI-H2100-250.2	2100	850	750	250	650	200	120	250	250	200	40	50	250

(Source: Precast concrete product brochure "Manufacturer A", 2024)

Table 2. Cross section of "Manufacturer B" I-girder

Cross section code	H mm	A mm	B mm	Tw1 mm	Tw2 mm	h1 mm	h2 mm	h3 mm	h4 mm	h5 mm	h6 mm	h7 mm	h8 mm
TYPE-1													
B-PCI-H900-170	900	550	650	170	550	150	75	100	125	-	-	21	125
B-PCI-H1250-170	1250	550	650	170	550	150	75	100	175	-	-	21	175
TYPE-2													
B-PCI-H1400-180	1400	700	650	180	550	200	120	100	225	200	22	21	225
B-PCI-H1600-180	1600	700	650	180	550	200	120	100	225	200	22	22	225
B-PCI-H1700-200	1700	800	700	200	600	200	120	250	250	250	40	50	250
B-PCI-H1850-200	1850	800	700	200	600	200	120	250	250	250	40	50	250
B-PCI-H2100-200	2100	800	700	200	600	200	120	250	250	250	40	50	250
B-PCI-H2300-200	2300	850	750	250	600	200	120	250	250	250	40	50	250

(Source: Precast concrete product brochure "Manufacturer B", 2024)

Data Analysis

This study analyzes PCI-girder bridges with span variations ranging from 20 to 45 meters, designed using the following technical specifications. The bridges are intended for toll road applications, with a lane width of 3.60 meters and two traffic lanes. The outer roadside width is 3.00 meters, while the inner width is 1.50 meters. The barriers have a width of 0.40 meters. The total roadway width is 11.70 meters, and the total slab width is 12.50 meters. The bridges have a skew angle of 0 degrees, a slab thickness of 250 mm, a deck slab thickness of 100 mm, and an asphalt thickness of 50 mm. The designed service life is 50 years. Girder spacing options include 1850 mm, 2100 mm, and 2450 mm. The reinforced concrete unit weight is 2500 kg/m³, with an ultimate tensile strength (f_{pu}) of strands at 1860 MPa. According to Setiawan et al. (2014), a jacking force of 75% f_{pu} produces almost linear stiffness behavior, therefore, a jacking force of 75% f_{pu} was also used in the research analysis. The beam's compressive strength ($f'_{c\ girder}$) ranges from 40 to 70 MPa, and the slab compressive strength ($f'_{c\ slab}$) is either 30 or 35 MPa.

The variation in girder spacing affects the number of girders used. For the 1850 mm center-to-center (CTC) spacing variant, seven girders are used, as shown in **Figure 4**; for the 2100 mm CTC spacing, six girders are used, as shown in **Figure 5**; and for the 2450 mm CTC spacing, five girders are used, as shown in **Figure 6**. Meanwhile, the cross-sections used for each span are adjusted based on the requirements to achieve optimal results while meeting design criteria. The cross-sections and concrete grades used in this study are presented in **Table 3**.

pISSN 2302-4240
eISSN 2655-2086
Volume 14, Issue 4, December 2025, pp.01074-01090
DOI: http://dx.doi.org/10.32832/astonjadro.v14i4.19037 http://ejournal.uika-bogor.ac.id/index.php/ASTONJADRO

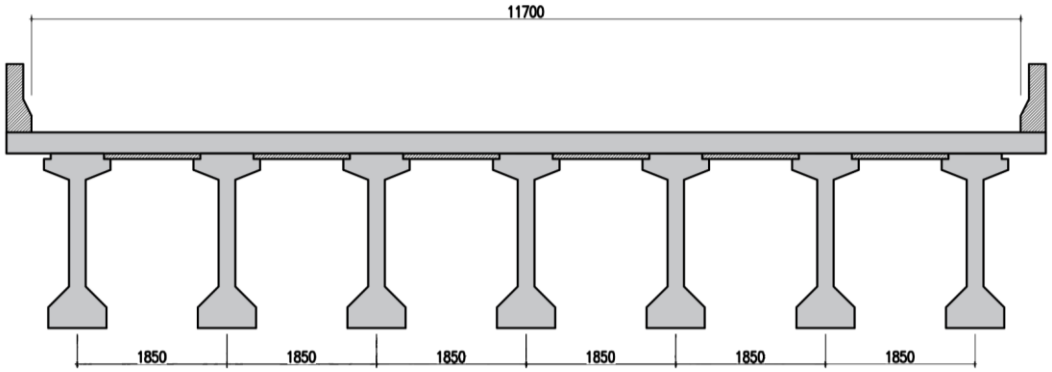

Figure 4. Cross section of the CTC 1850 mm bridge

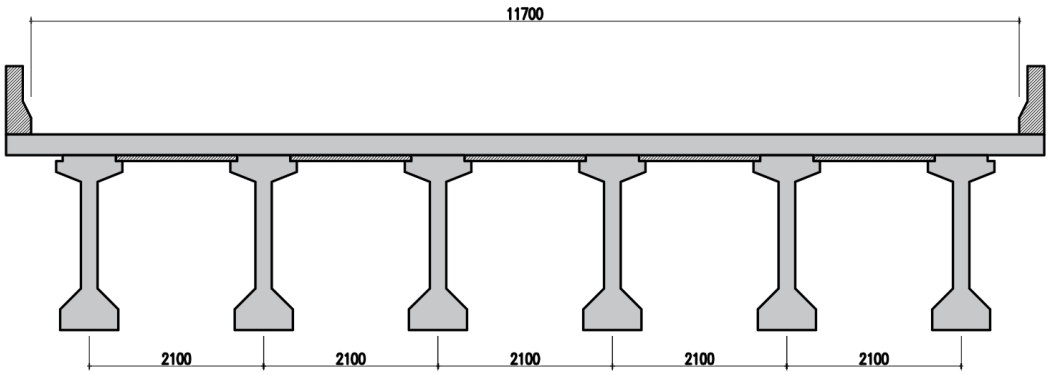

Figure 5. Cross section of the CTC 2100 mm bridge

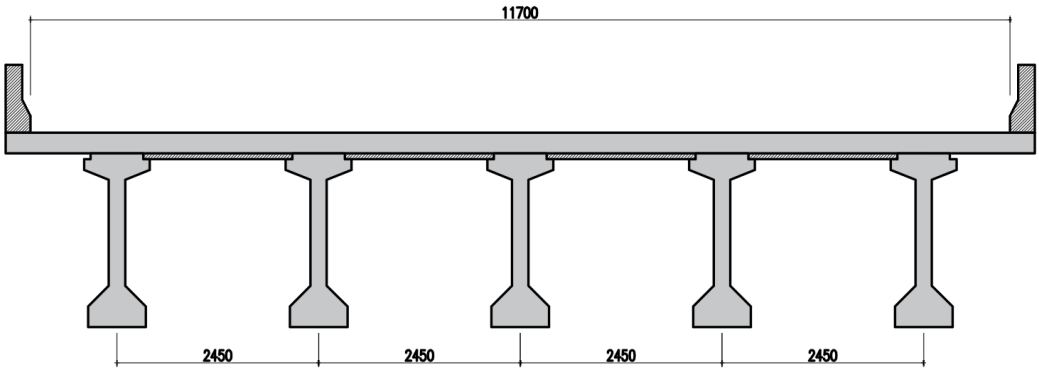

Figure 6. Cross section of the CTC 2450 mm bridge

Table 3. Section property & material

Span	Model variants	Cross section code	CTC	Beam height	f'c girder	f'c slab	Number of girders
m		(Tabel 3.1 & 3.2)	mm	mm	MPa	MPa	unit
20	1-a	B-PCI-1400.180	1850	1400	40	30	7
	1-b	B-PCI-1400.180	2100	1400	40	30	6
	1-c	B-PCI-1400.180	2450	1400	40	30	5
25	2-a	B-PCI-1600.180	1850	1600	40	30	7
	2-b	B-PCI-1600.180	2100	1600	40	30	6
	2-c	B-PCI-1600.180	2450	1600	40	30	5

Span	Model variants	Cross section code	CTC	Beam height	f'c girder	f'c slab	Number of girders
m		(Tabel 3.1 & 3.2)	mm	mm	MPa	MPa	unit
	3-a	A-PCI-1700.200.1	1850	1700	40	30	7
30	3-b	A-PCI-1700.200.1	2100	1700	40	30	6
	3-c	A-PCI-1700.200.1	2450	1700	45	30	5
	4-a	B-PCI-1850.200	1850	1850	40	30	7
35	4-b	B-PCI-1850.200	2100	1850	45	30	6
	4-c	B-PCI-1850.200	2450	1850	50	30	5
	5-a	A-PCI-2100.200.1	1850	2100	45	30	7
40	5-b	A-PCI-2100.200.1	2100	2100	50	30	6
	5-c	A-PCI-2100.200.1	2450	2100	55	30	5
	6-a	A-PCI-2100.200.1	1850	2100	55	30	7
45	6-b	A-PCI-2100.200.1	2100	2100	60	30	6
	6-c	A-PCI-2100.200.1	2450	2100	70	35	5

RESULT AND DISCUSSION

The cross-sectional capacity analysis using construction stage analysis requires the girder to behave as non-composite and composite with the slab during the construction stages. This affects the cross-sectional properties of both the edge and middle girders. The cross-sectional properties used in this study are presented in **Table 4** and **Table 5**.

Table 4. Edge beam section properties

Span	Model variants	Non-composite			Composite		
		Area	Yb	Ix	Area	Yb	Ix
m		mm^2	mm	mm^4	mm^2	mm	mm^4
	1-a	811200	694.8	138939450824	1211737	969.2	325830408688
20	1-b	811200	694.8	138939450824	1265863	993.0	342116103276
	1-c	811200	694.8	138939450824	1341641	1023.0	362746691547
	2-a	921250	794.8	205972993173	1321787	1076.6	449631014424
25	2-b	921250	794.8	205972993173	1375913	1102.2	471770454690
	2-c	921250	794.8	205972993173	1451691	1134.7	500027396602
	3-a	1077500	851.4	274719835701	1478037	1115.3	553562843439
30	3-b	1077500	851.4	274719835701	1532163	1140.3	580146155845
	3-c	1077500	851.4	274719835701	1577604	1160.1	601070021747
	4-a	1167500	926.5	352082166782	1568037	1194.3	682027425623
35	4-b	1167500	926.5	352082166782	1596161	1208.1	699012334461
	4-c	1167500	926.5	352082166782	1641940	1229.5	725426421172
	5-a	1317500	1051.6	510706874865	1695130	1313.0	916818209975
40	5-b	1317500	1051.6	510706874865	1724163	1328.3	940712856116
	5-c	1317500	1051.6	510706874865	1769861	1351.5	976944312543
	6-a	1317500	1051.6	510706874865	1659079	1293.2	885991850368
45	6-b	1317500	1051.6	510706874865	1688731	1309.5	911442362675
	6-c	1317500	1051.6	510706874865	1750603	1341.9	961787532947

Table 5. Middle beam section properties

Span	Model variants	Non-composite			Composite		
		Area	Yb	Ix	Area	Yb	Ix
m		mm^2	mm	mm^4	mm^2	mm	mm^4
	1-a	490750	679.3	118489048064	891287	1059.4	278303641294
20	1-b	490750	679.3	118489048064	945413	1086.0	289649672171
	1-c	490750	679.3	118489048064	1021191	1118.6	303563689651

pISSN 2302-4240
eISSN 2655-2086
Volume 14, Issue 4, December 2025, pp.01074-01090
DOI: http://dx.doi.org/10.32832/astonjadro.v14i4.19037 http://ejournal.uika-bogor.ac.id/index.php/ASTONJADRO

Span	Model variants	Non-composite			Composite		
		Area	Yb	Ix	Area	Yb	Ix
m		mm^2	mm	mm^4	mm^2	mm	mm^4
	2-a	526750	777.0	168059313265	927287	1186.5	374636738190
25	2-b	526750	777.0	168059313265	981413	1216.2	389750510197
	2-c	526750	777.0	168059313265	1057191	1252.6	408358309962
	3-a	669500	816.6	236410849044	1070037	1194.1	493336531357
30	3-b	669500	816.6	236410849044	1124163	1224.4	514127997660
	3-c	669500	816.6	236410849044	1169604	1247.8	530117244093
	4-a	699500	888.1	295225204696	1100037	1283.9	598171765063
35	4-b	699500	888.1	295225204696	1128161	1301.1	611416571985
	4-c	699500	888.1	295225204696	1173940	1327.4	631634021779
	5-a	749500	1008.0	410870326130	1127130	1415.8	784743224524
40	5-b	749500	1008.0	410870326130	1156163	1436.1	803430622612
	5-c	749500	1008.0	410870326130	1201861	1466.1	831029898632
	6-a	749500	1008.0	410870326130	1091079	1389.0	760166272525
45	6-b	749500	1008.0	410870326130	1120731	1411.1	780495622787
	6-c	749500	1008.0	410870326130	1182603	1453.7	819656635241

Using higher concrete grades and larger strand areas per girder unit is one of the effects of varying the spacing between girders. However, when multiplied by the total number of girders used in the bridge, the overall weight and volume decrease as the girder spacing increases. The concrete weight and strand areas used in this study are presented in **Table 6**, **Figure 7**, and **Figure 8**.

Table 6. Girder concrete weight & strand effective area

Span	Model variants	Weight of 1 girder	Weight of N girders	Number of strands in 1 girder	Effective strands area on N girder	Girder concrete volume
m		ton	ton	pcs	mm^2	m^3
	1-a	28.33	198.32	24	23520	79.33
20	1-b	28.33	169.99	26	21840	68.00
	1-c	28.33	141.66	30	21000	56.66
	2-a	37.59	263.16	30	29400	105.26
25	2-b	37.59	225.57	32	26880	90.20
	2-c	37.59	187.97	35	24500	75.19
	3-a	55.06	385.44	42	41160	154.18
30	3-b	55.06	330.38	44	36960	132.15
	3-c	55.06	275.31	48	33600	110.13
	4-a	66.77	467.38	51	49980	186.95
35	4-b	66.77	400.61	54	45360	160.25
	4-c	66.77	333.84	59	41300	133.54
	5-a	81.70	571.90	59	57820	228.76
40	5-b	81.70	490.20	62	52080	196.08
	5-c	81.70	408.50	67	46900	163.40
	6-a	91.07	637.48	74	72520	254.99
45	6-b	91.07	546.41	78	65520	218.57
	6-c	91.07	455.34	84	58800	182.14

Based on the cross-sectional specifications and materials mentioned above, these serve as references for theoretical and numerical analysis. Examples of numerical modeling using Midas Civil can be seen in **Figure 9**, **Figure 10**, and **Figure 11**.

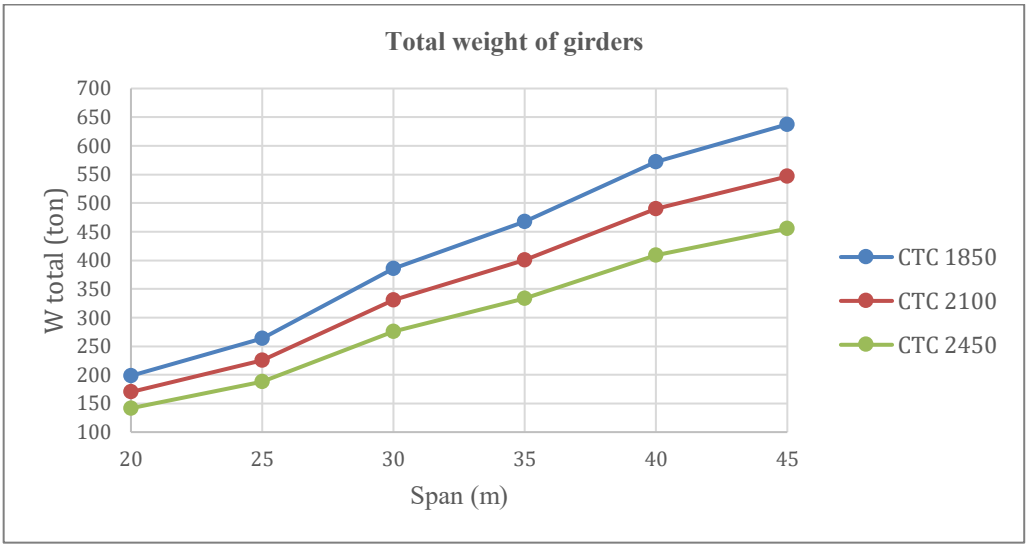

Figure 7. Total weight of girders

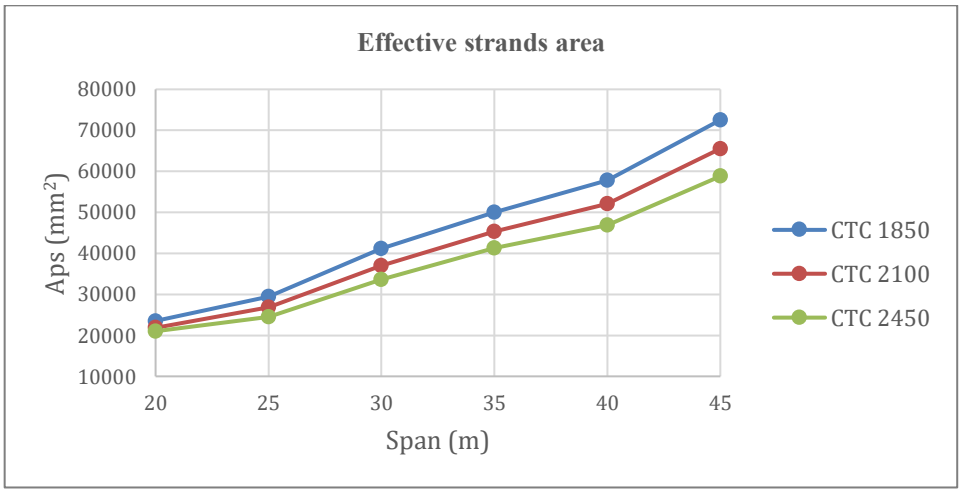

Figure 8. Effective strands area

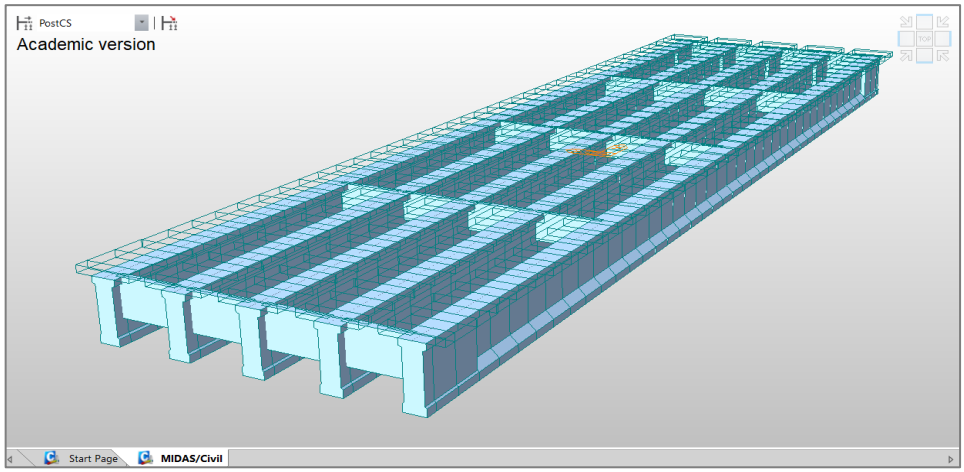

Figure 9. The 3D perspective of modeling girders and diaphragms in Midas Civil

pISSN 2302-4240
eISSN 2655-2086
Volume 14, Issue 4, December 2025, pp.01074-01090
DOI: http://dx.doi.org/10.32832/astonjadro.v14i4.19037 http://ejournal.uika-bogor.ac.id/index.php/ASTONJADRO

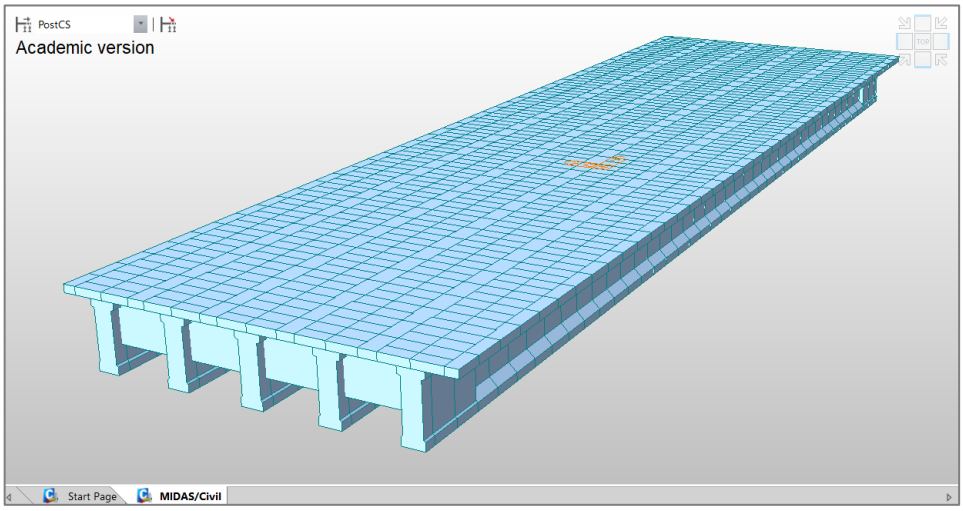

Figure 10. The 3D perspective of modeling all bridge elements in Midas Civil

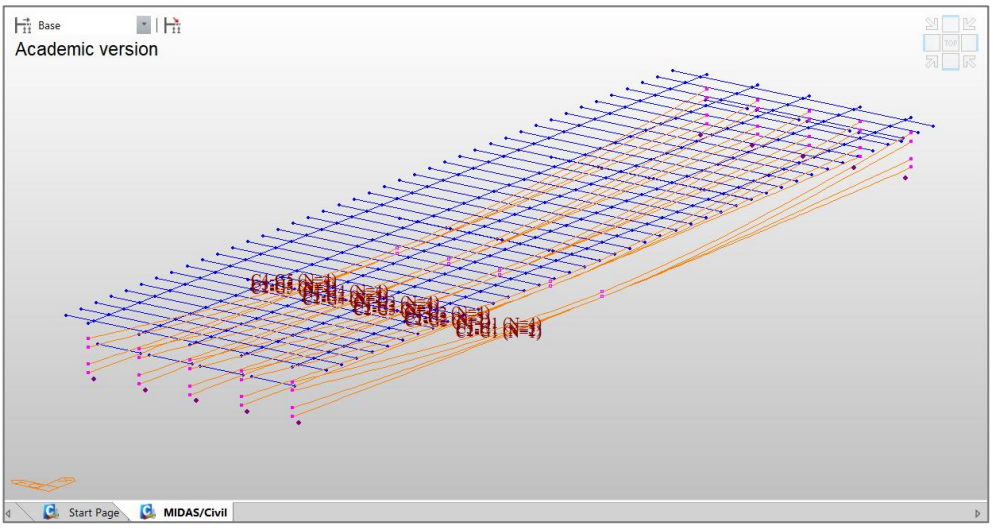

Figure 11. The 3D perspective of modeling cable tendons in Midas Civil

According to Zhang et al. (2009), modeling the bridge slab as a load on the girder during the construction period and then integrating it into a composite section with the girder once the concrete has hardened results in the section behaving as a perfectly elastic element during deformation due to the effects of creep and shrinkage. This study also employs the construction stage analysis method in both theoretical calculations and numerical analysis, as illustrated in **Figures 9** and **10**.

The load calculations to determine the ultimate moment on the girder refer to SNI 1725-2016 and Circular Letter No. 06/SE/Db/2021 from the Directorate General of Highways, which includes permanent loads in **Table 7** and transient loads in **Table 8**. Meanwhile, the calculation of moment and shear resistance for the girder follows SNI 2847-2019. The calculation results for the moment in this study are presented in **Table 9**, **Figure 11**, and **Figure 12**, while the shear resistance calculation results can be found in **Table 10**.

Table 7. Permanent load

Span	Model variants	Beam girder	Edge diaph.	Middle diaph.	Deck slab	Slab	Asphalt	Barrier
m		kN/m	kN	kN	kN/m	kN/m	kN/m	kN/m
	1-a	12.03	9.19	7.58	2.15	11.34	2.00	2.80

Span	Model variants	Beam girder	Edge diaph.	Middle diaph.	Deck slab	Slab	Asphalt	Barrier
m		kN/m	kN	kN	kN/m	kN/m	kN/m	kN/m
20	1-b	12.03	11.03	8.73	2.57	12.87	2.27	3.27
	1-c	12.03	13.97	10.43	3.17	15.02	2.64	3.92
	2-a	12.91	9.19	7.58	2.15	11.34	2.00	2.80
25	2-b	12.91	11.03	8.73	2.57	12.87	2.27	3.27
	2-c	12.91	13.97	10.43	3.17	15.02	2.64	3.92
	3-a	16.41	9.19	7.58	1.97	11.34	2.00	2.80
30	3-b	16.41	11.03	8.73	2.40	12.87	2.27	3.27
	3-c	16.41	13.61	10.34	3.00	15.02	2.64	3.92
	4-a	17.15	9.19	7.58	1.97	11.34	2.00	2.80
35	4-b	17.15	11.03	8.73	2.40	12.87	2.27	3.27
	4-c	17.15	13.61	10.34	3.00	15.02	2.64	3.92
	5-a	18.37	9.19	7.58	1.97	11.34	2.00	2.80
40	5-b	18.37	11.03	8.73	2.40	12.87	2.27	3.27
	5-c	18.37	13.61	10.34	3.00	15.02	2.64	3.92
	6-a	18.37	9.19	7.58	1.97	11.34	2.00	2.80
45	6-b	18.37	11.03	8.73	2.40	12.87	2.27	3.27
	6-c	18.37	13.61	10.34	3.00	15.02	2.64	3.92

Table 8. Transient load

Span	Model variants	Dynamic load allowance	Knife edge load	Distribution factor	Uniform distribution load	Live load	
						P KEL	q UDL
m			kN/m		kPa	kN	kN/m
	1-a	1.40	49.00	1.00	9.00	126.91	16.65
20	1-b	1.40	49.00	1.00	9.00	144.06	18.90
	1-c	1.40	49.00	1.00	9.00	168.07	22.05
	2-a	1.40	49.00	1.00	9.00	126.91	16.65
25	2-b	1.40	49.00	1.00	9.00	144.06	18.90
	2-c	1.40	49.00	1.00	9.00	168.07	22.05
	3-a	1.40	49.00	1.00	9.00	126.91	16.65
30	3-b	1.40	49.00	1.00	9.00	144.06	18.90
	3-c	1.40	49.00	1.00	9.00	168.07	22.05
	4-a	1.40	49.00	1.00	8.36	126.91	15.46
35	4-b	1.40	49.00	1.00	8.36	144.06	17.55
	4-c	1.40	49.00	1.00	8.36	168.07	20.48
	5-a	1.40	49.00	1.00	7.88	126.91	14.57
40	5-b	1.40	49.00	1.00	7.88	144.06	16.54
	5-c	1.40	49.00	1.00	7.88	168.07	19.29
	6-a	1.40	49.00	1.00	7.50	126.91	13.88
45	6-b	1.40	49.00	1.00	7.50	144.06	15.75
	6-c	1.40	49.00	1.00	7.50	168.07	18.38

Table 9. Moment ultimate and resistance

Span	Model variants	Factored flexural moment using theoretical calculations (Mu_1)	Factored flexural moment using numerical analysis (Mu_2)	Factored moment resistance (ϕMn)	Ratio $\phi Mn / Mu_1$	Ratio $\phi Mn / Mu_2$
m		kNm	kNm	kNm	> 1.0	> 1.0

pISSN 2302-4240
eISSN 2655-2086
Volume 14, Issue 4, December 2025, pp.01074-01090
DOI: http://dx.doi.org/10.32832/astonjadro.v14i4.19037 http://ejournal.uika-bogor.ac.id/index.php/ASTONJADRO

	1-a	5112.78	5671.4	6777.66	1.326	1.195
20	1-b	5579.17	6142.1	7344.34	1.316	1.196
	1-c	6330.66	6869.2	8400.28	1.327	1.223
	2-a	7318.88	7920.2	9555.87	1.306	1.207
25	2-b	7979.39	8724.5	10219.39	1.281	1.171
	2-c	9034.64	9789.2	11261.57	1.246	1.150
	3-a	10231.90	10777.5	13989.11	1.367	1.298
30	3-b	11352.42	12526.5	14740.26	1.298	1.177
	3-c	12921.16	13815.8	16236.77	1.257	1.175
	4-a	13374.67	14500.8	18196.15	1.360	1.255
35	4-b	14806.52	16370.1	19402.55	1.310	1.185
	4-c	16811.12	17875.9	21370.68	1.271	1.195
	5-a	17084.29	18435.0	23679.91	1.386	1.285
40	5-b	18862.23	20867.1	25150.51	1.333	1.205
	5-c	21351.33	22793.4	27480.25	1.287	1.206
	6-a	20959.71	22282.7	28893.92	1.379	1.297
45	6-b	23119.96	25114.3	30818.86	1.333	1.227
	6-c	26144.30	27534.9	34238.75	1.310	1.244

Table 10. Ultimate shear force and shear capacity

Span	**Model variants**	**Ultimate shear force using theoretical calculations (Vu_1)**	**Ultimate shear force using numerical analysis (Vu_2)**	**Shear capacity (ϕVnh)**	**Ratio $\phi Vnh/Vu_1$**	**Ratio $\phi Vnh/Vu_1$**
m		**kN**	**kN**	**kN**	**> 1.0**	**> 1.0**
	1-a	936.95	1234.0	2604.30	2.780	2.110
20	1-b	1047.09	1292.1	2604.30	2.487	2.016
	1-c	1201.28	1341.8	2604.30	2.168	1.941
	2-a	1123.57	1493.2	3069.82	2.732	2.056
25	2-b	1252.97	1536.7	3069.82	2.450	1.998
	2-c	1434.12	1629.6	3069.82	2.141	1.884
	3-a	1359.32	1780.3	3570.89	2.627	2.006
30	3-b	1507.98	1829.3	3570.89	2.368	1.952
	3-c	1716.10	1926.5	3570.89	2.081	1.854
	4-a	1523.32	2038.8	3942.16	2.588	1.934
35	4-b	1686.17	2164.2	3942.16	2.338	1.822
	4-c	1914.16	2339.7	3942.16	2.059	1.685
	5-a	1703.50	2354.7	4552.95	2.673	1.934
40	5-b	1880.55	2366.0	4552.95	2.421	1.924
	5-c	2128.41	2384.6	4552.95	2.139	1.909
	6-a	1857.94	2320.9	4557.78	2.453	1.964
45	6-b	2049.18	2464.5	4557.78	2.224	1.849
	6-c	2316.92	2587.1	4557.78	1.967	1.762

Table 11. Moment and shear due to live load.

Span	**Model variants**	**Moment due to live load (M_{LL})**	**Moment due to dead load (M_{DL})**	**Shear force due to live load (V_{LL})**	**Shear force due to dead load (V_{DL})**	**Ratio M_{LL}/M_{DL}**	**Ratio V_{LL}/V_{DL}**
m		**kNm**	**kNm**	**kN**	**kN**		
	1-a	1653.20	1592.32	293.41	314.63	1.038	0.933

Span m	Model variants	Moment due to live load (M_{LL}) kNm	Moment due to dead load (M_{DL}) kNm	Shear force due to live load (V_{LL}) kN	Shear force due to dead load (V_{DL}) kN	Ratio M_{LL}/M_{DL}	Ratio V_{LL}/V_{DL}
20	1-b	1840.33	1738.71	333.06	343.33	1.058	0.970
	1-c	2104.14	1943.64	388.57	383.51	1.083	1.013
	2-a	2140.02	2534.88	335.04	401.44	0.844	0.835
25	2-b	2437.84	2760.30	380.31	436.88	0.883	0.871
	2-c	2787.31	3075.89	443.70	486.51	0.906	0.912
	3-a	2824.95	3997.45	376.66	529.20	0.707	0.712
30	3-b	3206.70	4318.19	427.56	571.39	0.743	0.748
	3-c	3741.15	4767.23	498.82	630.46	0.785	0.791
	4-a	3477.88	5333.37	397.47	628.38	0.629	0.633
35	4-b	3947.87	5966.87	451.19	677.31	0.662	0.666
	4-c	4605.85	6573.77	526.38	745.82	0.701	0.706
	5-a	4182.85	7448.26	418.29	741.03	0.562	0.564
40	5-b	4748.10	8010.81	474.81	796.71	0.593	0.596
	5-c	5539.45	8798.37	553.95	874.67	0.630	0.633
	6-a	4939.85	9407.27	439.10	832.24	0.525	0.528
45	6-b	5607.39	10116.30	498.81	894.67	0.554	0.557
	6-c	6541.96	11108.94	581.51	982.06	0.589	0.592

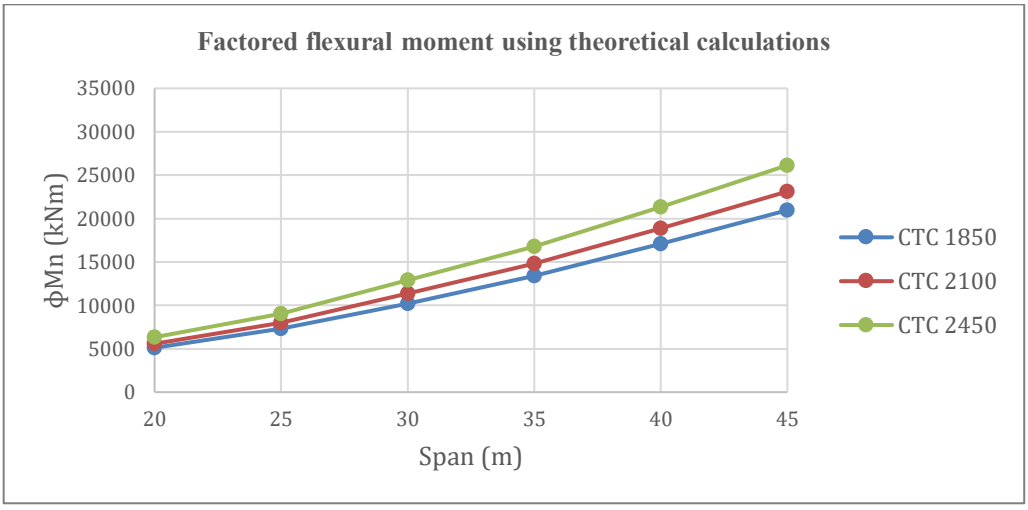

Figure 11. Factored flexural moment using theoretical calculations

pISSN 2302-4240
eISSN 2655-2086
Volume 14, Issue 4, December 2025, pp.01074-01090
DOI: http://dx.doi.org/10.32832/astonjadro.v14i4.19037 http://ejournal.uika-bogor.ac.id/index.php/ASTONJADRO

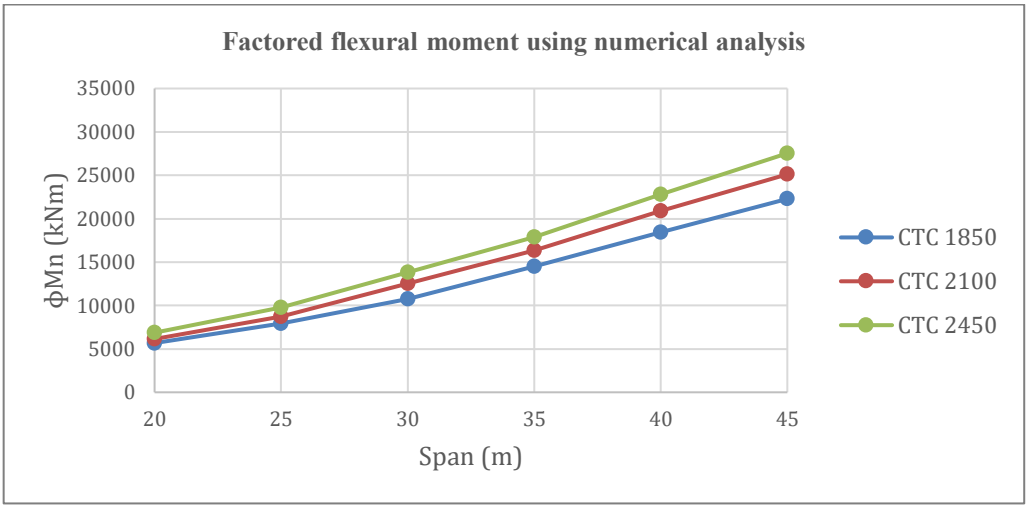

Figure 12. Factored flexural moment using numerical analysis

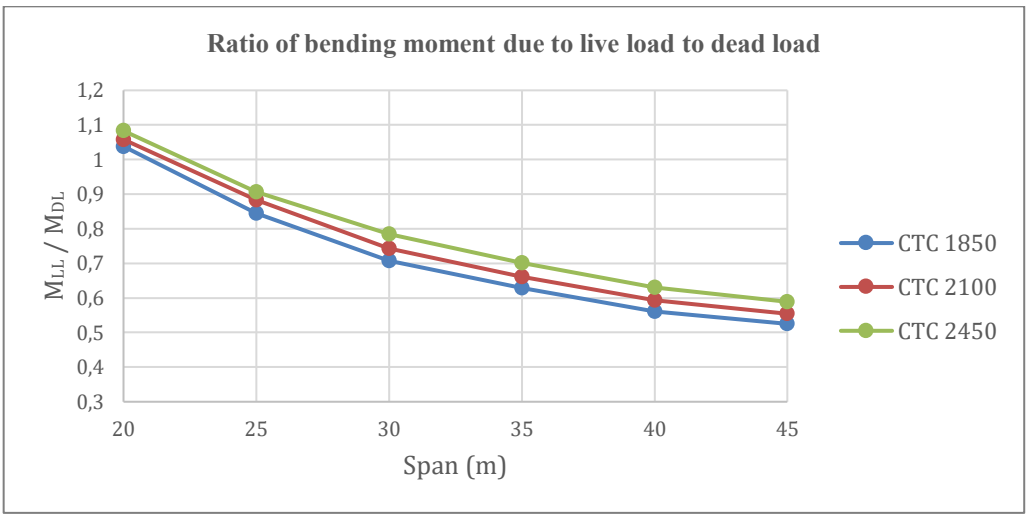

Figure 13. The ratio of bending moment due to live load to dead load

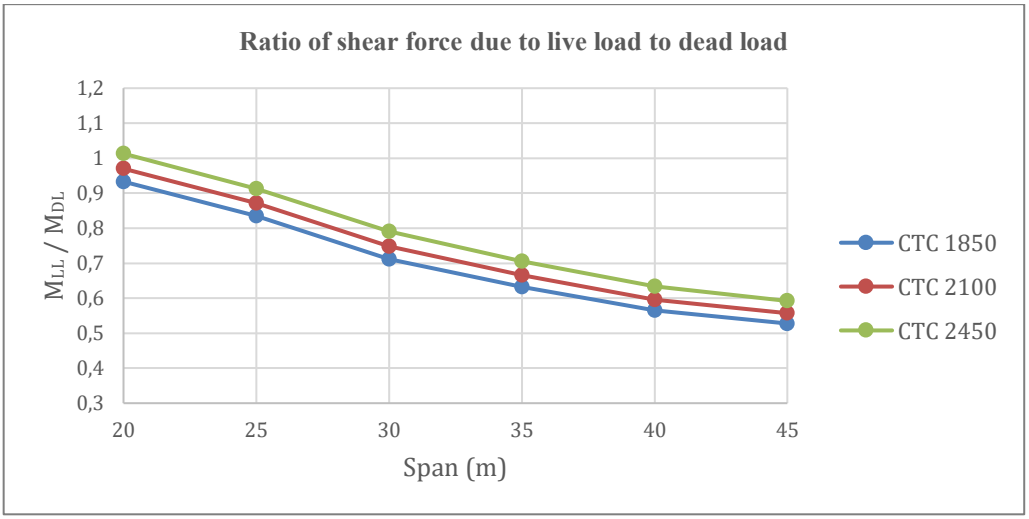

Figure 14. The ratio of shear force due to live load to dead load

According to Hatem et al. (2014), the moment and shear force ratio from live load to dead load in I-girder bridges decreases as the span increases. However, bridges with spans exceeding 30 meters exhibit moments and shear forces due to live load greater than those due to dead load. Similar calculations were conducted in this study, with the resulting ratios of M_{LL}/M_{DL} and V_{LL}/V_{DL} shown in **Table 11**, **Figure 13**, and **Figure 14**.

The prestress loss in the girder must be analyzed for short-term (post-tension) and long-term losses. This analysis will determine the stress on the beam surface, which must comply with the allowable concrete stress as specified in Equations (1), (2), (3), and (4) for the initial condition, as well as Equations (5) and (6) for the service condition, as outlined in **Table 12**.

Table 12. Beam stress control at mid-span

Span	Model variants	Initial condition		Service condition		
		σ top	σ bottom	σ slab	σ top	σ bottom
m		N/mm²	N/mm²	N/mm²	N/mm²	N/mm²
	1-a	0.1 > -1.6	15.9 < 24.0	6.1 < 13.5	9.4 < 18.0	1.4 > -3.2
20	1-b	-0.1 > -1.6	17.4 < 24.0	6.2 < 13.5	9.9 < 18.0	1.3 > -3.2
	1-c	-0.3 > -1.6	20.3 < 24.0	6.5 < 13.5	12.9 < 18.0	0.7 > -3.2
	2-a	0.3 > -1.6	18.7 < 24.0	6.7 < 13.5	11.4 < 18.0	1.5 > -3.2
25	2-b	0.02 > -1.6	20.2 < 24.0	6.8 < 13.5	12.1 < 18.0	1.1 > -3.2
	2-c	-0.6 > -1.6	22.7 < 24.0	7.1 < 13.5	12.9 < 18.0	0.7 > -3.2
	3-a	0.7 > -1.6	20.3 < 24.0	7.2 < 13.5	13.0 < 18.0	2.5 > -3.2
30	3-b	0.5 > -1.6	21.5 < 24.0	7.6 < 13.5	13.9 < 18.0	1.6 > -3.2
	3-c	-0.2 > -1.6	24.2 < 27.0	8.4 < 13.5	15.1 < 20.3	1.1 > -3.4
	4-a	1.0 > -1.6	23.6 < 24.0	7.9 < 13.5	15.3 < 18.0	2.8 > -3.2
35	4-b	0.7 > -1.7	25.3 < 27.0	8.6 < 13.5	16.6 < 20.3	2.1 > -3.4
	4-c	-0.02 > -1.8	28.4 < 30.0	9.5 < 13.5	18.1 < 22.5	1.5 > -3.5
	5-a	1.2 > -1.7	25.5 < 27.0	8.2 < 13.5	16.4 < 20.3	3.6 > -3.4
40	5-b	0.8 > -1.8	27.2 < 30.0	8.9 < 13.5	17.7 < 22.5	2.9 > -3.5
	5-c	-0.05 > -1.9	30.2 < 33.0	9.8 < 13.5	19.2 < 24.8	2.1 > -3.7
	6-a	1.5 > -1.9	24.8 < 33.0	10.4 < 13.5	20.9 < 24.8	4.4 > -3.7
45	6-b	1.0 > -1.9	34.4 < 36.0	11.3 < 13.5	22.6 < 27.0	3.5 > -3.9
	6-c	0.03 > -2.1	38.0 < 42.0	12.0 < 15.8	24.2 < 31.5	2.7 > -4.2

During the post-tensioning process, the beam will experience camber within the limits defined by Equation (11), while the deflection caused by the live load must comply with the constraints specified in Equation (14). The calculated results for camber and deflection in this study are presented in **Table 13**.

Table 13. Beam camber & deflection at mid-span

Span	Model variants	Camber at applied prestress	Deflection due to live load using theoretical calculations	Deflection due to live load using numerical analysis	Allowable deflection resulting from live load
m		mm	mm	mm	mm
	1-a	- 11.47 (↑)	4.80 (↓)	5.06 (↓)	
20	1-b	- 12.83 (↑)	4.87 (↓)	5.17 (↓)	25.00 (↓)
	1-c	- 14.95 (↑)	6.71 (↓)	7.04 (↓)	
	2-a	- 19.62 (↑)	6.70 (↓)	7.23 (↓)	
25	2-b	- 21.55 (↑)	6.88 (↓)	7.37 (↓)	31.25 (↓)
	2-c	- 24.98 (↑)	11.04 (↓)	12.11 (↓)	
	3-a	- 27.85 (↑)	10.81 (↓)	10.86 (↓)	
30	3-b	- 31.02 (↑)	12.10 (↓)	10.97 (↓)	37.50 (↓)
	3-c	- 34.17 (↑)	14.69 (↓)	17.94 (↓)	

pISSN 2302-4240
eISSN 2655-2086
Volume 14, Issue 4, December 2025, pp.01074-01090
DOI: http://dx.doi.org/10.32832/astonjadro.v14i4.19037 http://ejournal.uika-bogor.ac.id/index.php/ASTONJADRO

Span	Model variants	Camber at applied prestress	Deflection due to live load using theoretical calculations	Deflection due to live load using numerical analysis	Allowable deflection resulting from live load
m		mm	mm	mm	mm
	4-a	- 40.60 (↑)	14.17 (↓)	15.05 (↓)	
35	4-b	- 43.17 (↑)	16.03 (↓)	14.58 (↓)	43.75 (↓)
	4-c	- 47.69 (↑)	18.95 (↓)	24.14 (↓)	
	5-a	- 46.97 (↑)	16.42 (↓)	17.03 (↓)	
40	5-b	- 50.58 (↑)	18.68 (↓)	16.53 (↓)	50.00 (↓)
	5-c	- 55.96 (↑)	21.88 (↓)	27.69 (↓)	
	6-a	- 68.46 (↑)	22.34 (↓)	23.81 (↓)	
45	6-b	- 74.27 (↑)	25.70 (↓)	23.21 (↓)	56.25 (↓)
	6-c	- 79.11 (↑)	26.87 (↓)	37.45 (↓)	

CONCLUSION

The conclusions that can be drawn from this research are in terms of cross-sectional properties, the spacing between girders significantly impacts the increase in the effective area of the girder when the section functions as a composite with the slab, due to the enlargement of the effective width. Additionally, as the girder spacing increases, for the same span length and cross-sectional dimensions, a larger area of strands is required to achieve (1) the necessary camber and deflection as per design requirements, which necessitates higher concrete strength to accommodate (2) the beam stress on the top surface of the girder, particularly after the application of prestressing forces (post-tensioning). These two requirements are the most influential factors in the optimal design of PCI-Girder bridges. Camber must occur before live loads are applied to the bridge. Based on the results of moment calculations, for all variations of the distance between girders on bridges with spans above 20 meters, it shows that the ratio of moment due to live load to moment due to dead load is below 1, which means dead load is more dominant than live load. Meanwhile, the 20-meter span has a ratio above 1, or it can be interpreted that the live load is more dominant than the dead load. The moment and shear force ratios due to live load relative to dead load decrease as the bridge span length increases, regardless of girder spacing variations. This indicates that with longer spans, the influence of dead load becomes more significant compared to live load. The 2450 mm CTC spacing variant exhibits a higher M_{LL}/M_{DL} and V_{LL}/V_{DL} ratios compared to other variants.

REFERENCES

[1] Ministry of Public Works and Housing of the Republic of Indonesia. (2024). Informasi Statistik Infrastruktur PUPR 2023. Jakarta. Data and Information Technology Center, Ministry of Public Works and Housing.

[2] Tambunan, R., Aminullah, A., Sulistyo, D. (2022). Demand Analysis of Material, Construction Equipment, and Labor on the Superstructure of Type I-Girder Bridge. Inersia, 18-2.

[3] Mitoulis, S.A., Ioannis A. T., Kosmas C. S. (2010). Cost-effectiveness related to the earthquake resisting system of multi-span bridges. Engineering Structures, 32, 2658–2671.

[4] Mahmoud Jahjouh, Semih Erhan. (2022). Optimization of prestressed concrete bridge girder section using a modified harmony search algorithm. Structures, 46, 625–636.

[5] American Association of State Highway and Transportation Officials. (2020). AASHTO LRFD Bridge Design Specifications 9th Edition. Washington, DC 20004, USA. American Association of State Highway and Transportation Officials. ISBN: 978-1-56051-738-2.

[6] National Standardization Agency of Indonesia. (2004). SNI T-12-2004 on Design of Concrete Structures for Bridges. Jakarta: National Standardization Agency of Indonesia.

[7] National Standardization Agency of Indonesia. (2016). SNI 1725-2016 on Loading for Bridges. Jakarta: National Standardization Agency of Indonesia.

[8] Ministry of Public Works and Housing of the Republic of Indonesia. (2021). Circular Letter of the Directorate General of Highways No. 06/SE/Db/2021 concerning Guidelines for Roads and Bridges No. 02/M/BM/2021. Jakarta: Ministry of Public Works and Housing, Directorate General of Highways.

[9] Hatem M. Seliem, Mostafa Eid, Alaa G. Sherif. (2014). Assessment of vehicular live load and load factors for design of short-span bridges according to the new Egyptian Code. HBRC Journal.

[10] National Standardization Agency of Indonesia. (2019). SNI 2847-2019 on Structural Concrete Requirements for Buildings. Jakarta: National Standardization Agency of Indonesia.

[11] Precast/Prestressed Concrete Institute. 2010. PCI Design Handbook – Precast and Prestressed Concrete 7th Edition. Chicago, IL 60606-5230, USA. Precast/Prestressed Concrete Institute. ISBN 978-0-937040-87-4.

[12] Ministry of Public Works and Housing of the Republic of Indonesia. (2022). Informasi Statistik Infrastruktur PUPR 2022. Jakarta. Data and Information Technology Center, Ministry of Public Works and Housing.

[13] Ministry of Public Works and Housing of the Republic of Indonesia. (2023). Regulation of the Minister of Public Works and Housing of the Republic of Indonesia Number 05 of 2023 on Technical Requirements for Roads and Road Planning. Jakarta: Ministry of Public Works and Housing.

[14] Ministry of Public Works and Housing of the Republic of Indonesia. (2023). Laporan Kinerja 2022 Kementerian PUPR. Jakarta, Ministry of Public Works and Housing.

[15] Ministry of Public Works and Housing of the Republic of Indonesia. (2024). Laporan Kinerja 2023 Kementerian PUPR. Jakarta, Ministry of Public Works and Housing.

[16] Setiawan, A. F., Sulistyo, D., & Aminullah, A. (2014). Finite element method for numerical analysis of post-tension anchorage zone. Procedia Engineering, 95, 272–278.

[17] Zhang, J., Koo, M.-S., Jeong, Y.-D., & Aminullah, A. (2009). Simulation of composite deck-girder bridge by solid elements. IABSE Symposium on Sustainable Infrastructure - Environment Friendly, Safe and Resource Efficient, Bangkok, 9-11 September 2009.